



Cite this: *RSC Adv.*, 2019, 9, 3688

# Near-infrared light-driven photocatalytic NaYF<sub>4</sub>:Yb,Tm@ZnO core/shell nanomaterials and their performance

Junjie Zhang,<sup>ab</sup> Suling Zhao,<sup>ab</sup> Zheng Xu,<sup>ab</sup> Ligang Zhang,<sup>ab</sup> Pengfei Zuo<sup>ab</sup> and Qixiao Wu<sup>ab</sup>

Herein, the infrared-responsive photocatalyst NaYF<sub>4</sub>:Yb,Tm@ZnO has been successfully synthesized by combining semiconductor ZnO with an upconversion material, NaYF<sub>4</sub>:Yb,Tm. In this composite, NaYF<sub>4</sub>:Yb,Tm emits intense ultraviolet and blue upconversion luminescence upon excitation by a 980 nm laser and provides the necessary energy of ultraviolet light to ZnO. The photocatalytic activity of NaYF<sub>4</sub>:Yb,Tm@ZnO composites has been studied using methylene blue by irradiation with a 980 nm laser, and the results indicate that the NaYF<sub>4</sub>:Yb,Tm@ZnO composite is an advanced near-infrared-driven photocatalyst; this study presents a promising strategy to utilize the near-infrared-responsive upconversion materials for photocatalytic applications.

Received 21st September 2018  
 Accepted 26th December 2018

DOI: 10.1039/c8ra07861k

[rsc.li/rsc-advances](http://rsc.li/rsc-advances)

## Introduction

In recent years, environmental pollution has become a very serious problem,<sup>1</sup> and the application of photocatalysis for controlling environmental pollution has attracted significant attention of researchers from all over the world.<sup>2</sup> Ever since Fujishima and Honda discovered photocatalysis on the TiO<sub>2</sub> electrode for hydrogen production phenomenon in 1972,<sup>3</sup> TiO<sub>2</sub> photocatalysts have attracted the attention of researchers due to their oxidation ability, environmentally friendly nature and chemical stability under the irradiation of ultraviolet (UV) light;<sup>4–9</sup> however, UV radiation of the solar energy occupies only *ca.* 5%, whereas the energy in the visible light (*ca.* 48%) and near-infrared (NIR) light (*ca.* 47%) range is not used for photocatalysis.<sup>10,11</sup> To fully use the solar energy in the photocatalysis of semiconductors, several methods, such as semiconductor coupling<sup>12–14</sup> and impurity doping, have been proposed for extending the absorption range.<sup>15–17</sup> The semiconductor photocatalysis can be adjusted to the visible light region using these methods.<sup>18–20</sup> However, the efficiency of using long-wavelength light in the field of photocatalysis is still a challenge due to the poor absorption of photocatalytic materials.

Moreover, nanomaterials with upconversion (UC) luminescence have received extensive attention owing to their potential application in bio-analysis, medical therapy, optical devices, and photovoltaic cells.<sup>21</sup> To date, fluoride crystals have been regarded as one of the best UC matrices due to their low phonon

energy and high chemical stability. Note that a higher UC efficiency can be expected in rare earth ion (RE<sup>3+</sup>)-doped NaYF<sub>4</sub> crystals due to their unique optical properties arising from the intra 4f transitions.<sup>22</sup>

In the last decade, the focused NaYF<sub>4</sub>:Yb,Er/Tm agents have been successfully applied to advanced assembly materials. For example, the preparation of the NaYF<sub>4</sub>:Yb,Tm/CdS composite has been reported, and the NIR photocatalytic activity has been investigated by degrading Rhodamine B and methylene blue.<sup>23</sup> The NaYF<sub>4</sub>:Yb,Tm@TiO<sub>2</sub> core@shell photocatalyst has been successfully fabricated by a simple hydrothermal method followed by hydrolysis of titanium isopropoxide (TTIP) with polyvinylpyrrolidone K-30 (PVP) as the coupling agent; this study suggests a promising system to utilize the NIR energy of sunlight for photochemical and photoelectrical applications based on TiO<sub>2</sub>.<sup>24,25</sup> The NaYF<sub>4</sub>:Yb,Tm/g-C<sub>3</sub>N<sub>4</sub> (NYT/C<sub>3</sub>N<sub>4</sub>) photocatalyst has been successfully fabricated by a stepwise method to utilize the NIR energy of sunlight for photochemical and photoelectrical applications based on g-C<sub>3</sub>N<sub>4</sub>.<sup>26</sup> We have recently proposed the assembly of composites formed by NaYF<sub>4</sub>:Yb,Tm as a core and Cu<sub>2</sub>O as a shell that presents an interesting high performance for organic pollutant degradation under NIR irradiation.<sup>11</sup> The infrared-responsive photocatalysts of NaYF<sub>4</sub>:Yb,Tm@ZnO were synthesized by a two-step high-temperature thermolysis method.<sup>27</sup> In another method, the NaYF<sub>4</sub>:Yb, Tm@ZnO heterogeneous nanoparticles with an epitaxial interface have been prepared by carefully controlling the temperature. This heterogeneous core-shell structure facilitates the enhancement in both the upconversion luminescence and the ultrahigh photocurrent response by providing efficient energy transfer channels.<sup>28</sup> However, the photocatalytic

<sup>a</sup>Key Laboratory of Luminescence and Optical Information, Beijing Jiaotong University, Ministry of Education, Beijing 100044, China

<sup>b</sup>Institute of Optoelectronics Technology, Beijing Jiaotong University, Beijing 100044, China



activity of these prepared materials has not been comprehensively investigated.

Inspired by the abovementioned investigation, herein, a core-shell nanoparticle consisting of the upconversion luminescent  $\text{NaYF}_4:\text{Yb,Tm}$  and the n-type semiconductor ZnO for NIR responsive photocatalysis was synthesized. Compared with those reported in the previous study, the photocatalytic activities of the  $\text{NaYF}_4:\text{Yb,Tm}@ZnO$  composite were studied by the degradation of methylene blue in an aqueous solution upon NIR irradiation, and the degradation rate reached 68.7%. An important consequence was found that the  $\text{NaYF}_4:\text{Yb,Tm}@ZnO$  composite showed a significantly improved catalytic activity under NIR irradiation as compared to ZnO and the physical mixture of  $\text{NaYF}_4:\text{Yb,Tm}$  and ZnO.

## Experimental

$\text{YCl}_3 \cdot 6\text{H}_2\text{O}$  (99.999%),  $\text{YbCl}_3$  (99.998%),  $\text{TmCl}_3$  (99.995%), NaOH,  $\text{NH}_4\text{F}$ , oleic acid (OA), 1-octadecene (ODE) and zinc(II) acetylacetonate ( $\text{Zn}(\text{acac})_2$ ) were purchased from the Sigma-Aldrich (St. Louis, MO, USA) company and used without further purification.

$\text{NaYF}_4:20\%\text{Yb},2\%\text{Tm}$  nanoparticles were synthesized by a solvothermal method. Typically, 1 mmol  $\text{YCl}_3$ ,  $\text{YbCl}_3$ , and  $\text{TmCl}_3$  in a ratio of 78 : 20 : 2 were added to the mixture of 15 mL ODE and 6 mL OA in a 50 mL two-necked flask followed by heating to 160 °C to form a homogeneous solution. After being cooled down to room temperature, a 10 mL methanol solution containing NaOH (0.01 g) and  $\text{NH}_4\text{F}$  (0.148 g) was slowly added to the two-necked flask, and the mixture was stirred for 30 min and then heated slowly to 100 °C for another 30 min to remove water, oxygen and methanol. Subsequently, the solution was quickly heated up to 300 °C and maintained at this temperature for 1.5 h under an argon atmosphere. After the solution was cooled down naturally, samples were obtained by centrifugation and washed three times with ethanol.

ZnO-coated  $\text{NaYF}_4:\text{Yb,Tm}$  nanocomposites were prepared as follows: 0.1 mmol  $\text{NaYF}_4:\text{Yb,Tm}$  was mixed with benzyl ether (5 mL) in a round-bottom flask under stirring. After this, 0.02636 g (0.1 mmol)  $\text{Zn}(\text{acac})_2$  was mixed with a mixture of benzyl ether (10 mL) in a 50 mL round-bottom flask under stirring; then, the mixture was heated to 150 °C, maintained at this temperature for 1.5 h and then slowly added to the flask that contained  $\text{NaYF}_4:\text{Yb,Tm}$ ; then, the mixed solution was stirred for 30 min. After this, the solution was heated to 200 °C and maintained at this temperature for 1 h under an argon atmosphere; then, the mixture was heated to 250 °C and maintained at this temperature for 30 min under an argon atmosphere. After the solution was cooled down naturally, nanocrystals were obtained from the solution with ethanol and water by centrifugation, washed three times, dried at 60 °C for 12 h, and annealed at 400 °C for 2 h under an argon atmosphere.

Pure ZnO nanocrystals were prepared by the abovementioned procedures without the addition of  $\text{NaYF}_4:\text{Yb,Tm}$ , and the  $\text{NaYF}_4:\text{Yb,Tm}$  nanocrystals were also prepared by following the abovementioned procedures. Then, they were

mixed mechanically at the same molar ratio as used in the preparation of the  $\text{NaYF}_4:\text{Yb,Tm}@ZnO$  composites.

Photocatalysis of the products was monitored by means of degradation of methyl blue (MB). Then, 0.5 mg of the  $\text{NaYF}_4:\text{Yb,Tm}@ZnO$  nanocomposites were dispersed in a cuvette containing a MB aqueous solution (0.5 mL  $15 \text{ mg L}^{-1}$ ). Prior to irradiation, the aqueous solution was kept in dark for 5 h for establishing an adsorption-desorption equilibrium of MB on the surface of  $\text{NaYF}_4:\text{Yb,Tm}@ZnO$  nanocomposites before irradiation. A diode laser of 980 nm with a power of  $10 \text{ W cm}^{-2}$  was used as the irradiation source. After irradiation for 2 h, 0.3 mL of MB aqueous solution was taken out for UV-vis absorbance measurement and then put back into the quartz corvette.

The X-ray powder diffraction (XRD) analyses were performed using a Bruker D8 Advance X-ray diffractometer (Billerica, MA, USA) with  $\text{Cu K}\alpha 1$  irradiation ( $\lambda = 1.54056 \text{ \AA}$ ). The transmission electron microscopy (TEM) images were obtained using a JEOL JEM-1400 transmission electron microscope (Tokyo, Japan). The upconversion (UC) luminescence spectra were obtained using a ZOLIX fluorescence spectrometer system, and the excitation source used was an external 980 nm semiconductor laser (ZOLIX INSTRUMENTS CO. LTD) with an optic fiber accessory. The absorption of water was measured by a UV-3101PC UV-VIS-NIR scanning spectrophotometer (Shimadzu, Kyoto, Japan).

## Results and discussion

To determine the crystal structure of the as-synthesized products, the hexagonal phase  $\text{NaYF}_4:\text{Yb,Tm}$  NCs and  $\text{NaYF}_4:\text{Yb,Tm}@ZnO$  composite NCs were examined by XRD. Fig. 1a shows the XRD patterns of the prepared NCs. The diffraction peaks of the  $\text{NaYF}_4:\text{Yb,Tm}$  NCs could be indexed to a pure hexagonal phase  $\text{NaYF}_4$  structure (JCPDS 16-0334) very well, and no other phase can be identified. In addition to the XRD pattern of the hexagonal phase of  $\text{NaYF}_4$ , the characteristic diffraction peaks (100), (101) and (110) of ZnO (JCPDS 79-0208) can be observed in Fig. 1b. It should be concluded preliminarily that the composites of  $\text{NaYF}_4$  and ZnO have been synthesized.

The  $\text{NaYF}_4:\text{Yb,Tm}$  NCs and  $\text{NaYF}_4:\text{Yb,Tm}@ZnO$  composite products prepared by TEM are displayed in Fig. 2. In Fig. 2a,  $\text{NaYF}_4:\text{Yb,Tm}$  NCs show hexagonal appearance with a uniform

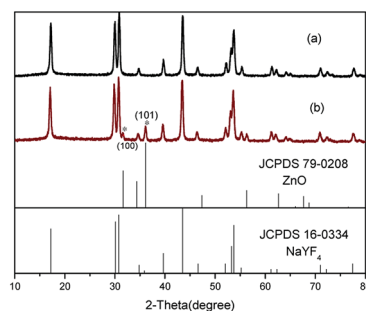


Fig. 1 XRD patterns of  $\text{NaYF}_4:\text{Yb,Tm}$  nanocrystals (a) and with ZnO coating (b). Standard XRD patterns of JCPDS 16-0334 ( $\text{NaYF}_4$ ) and 79-0208 (ZnO) are also shown.



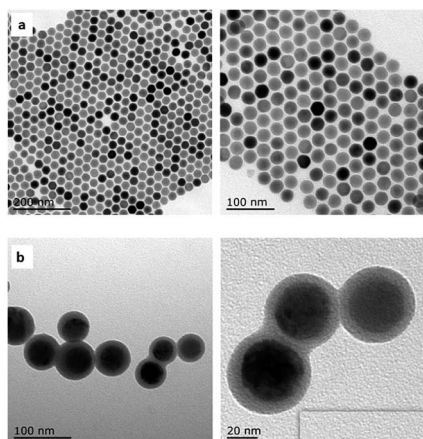


Fig. 2 TEM images of NaYF<sub>4</sub>:Yb,Tm nanocrystals (a) and core-shell NaYF<sub>4</sub>:Yb,Tm@ZnO nanoparticles (b).

size of 28 nm. After surface modification by ZnO, the average size of the NaYF<sub>4</sub>:Yb,Tm@ZnO composites increased to 31 nm, as shown in Fig. 2b. The thickness of the shell ZnO is about 5 nm.

NaYF<sub>4</sub>:Yb,Tm is a typical upconversion luminescent material for converting NIR excitation light to higher energies *via* successive energy transfer processes. Scheme in Fig. 3a illustrates the processes of upconversion luminescence in a Yb<sup>3+</sup>-Tm<sup>3+</sup> codoped system. Yb<sup>3+</sup> ions absorb the light of 980 nm, and some energy transfers from the excited Yb<sup>3+</sup> ions to the neighboring Tm<sup>3+</sup> ions, which are excited and then provide emissions.<sup>29</sup> The upconversion fluorescence spectra of NaYF<sub>4</sub>:Yb,Tm and photoluminescence emission spectra of NaYF<sub>4</sub>:Yb,Tm@ZnO composites under 980 nm excitation are shown in Fig. 3b. In the spectrum of NaYF<sub>4</sub>:Yb,Tm, three UV emission peaks located at 291 nm, 345 nm, and 361 nm, blue emission peaks at 451 nm and 476 nm and a red emission peak at 645 nm are attributed to the transitions of Tm<sup>3+</sup> ions corresponding to <sup>1</sup>I<sub>6</sub> → <sup>3</sup>H<sub>6</sub>, <sup>1</sup>I<sub>6</sub> → <sup>3</sup>F<sub>4</sub>, and <sup>1</sup>D<sub>2</sub> → <sup>3</sup>H<sub>6</sub>, <sup>1</sup>D<sub>2</sub> → <sup>3</sup>F<sub>4</sub> and <sup>1</sup>G<sub>4</sub> → <sup>3</sup>H<sub>6</sub> and <sup>1</sup>G<sub>4</sub> → <sup>3</sup>F<sub>4</sub>. The peaks of the upconversion luminescence

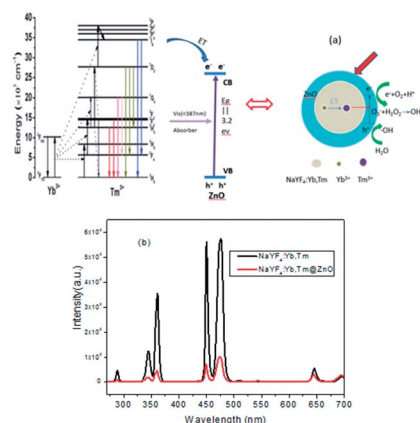


Fig. 3 (a) The upconversion luminescence processes in a Yb<sup>3+</sup>-Tm<sup>3+</sup> codoped system and working mechanism of NaYF<sub>4</sub>:Yb,Tm@ZnO nanoparticle under excitation at 980 nm. (b) Photoluminescence (PL) spectra of NaYF<sub>4</sub>:Yb,Tm and NaYF<sub>4</sub>:Yb,Tm@ZnO composites under 980 nm excitation at room temperature.

are same for two samples; this means that all emissions are from Tm<sup>3+</sup> ions. However, after the coating of ZnO, the upconversion intensity of NaYF<sub>4</sub>:Yb,Tm@ZnO is weaker than that of pure NaYF<sub>4</sub>:Yb,Tm obviously. Especially, upon coating with a ZnO layer, the intensities of the emissions at 291, 345 and 361 nm decrease significantly when compared with those of 451 and 476 nm that change less. Because the photon energies of 291, 345, and 361 nm are higher than the band gap of ZnO, the spectral change may be relevant to the presence of ZnO around the upconversion NaYF<sub>4</sub>:Yb,Tm particles according to the different decreasing ratios.

To ascertain the origin of photoluminescence spectral changes, the UV-vis absorption spectrum of NaYF<sub>4</sub>:Yb,Tm@ZnO was measured, as shown in Fig. 4. In the absorption band in the UV region, a peak starting at about 387 nm, corresponding to the band gap (3.2 eV) of ZnO semiconductor, overlaps with the emission spectra of 291, 345 and 361 nm. Therefore, we can speculate that the emission spectra of 291, 345 and 361 nm generated *via* the upconversion process of NaYF<sub>4</sub>:Yb,Tm has been absorbed partially by ZnO. Therefore, it is possible to realize the photocatalysis under near-infrared light using NaYF<sub>4</sub>:Yb,Tm@ZnO nanocomposites, as shown in Fig. 3a.

To judge the photocatalytic activity of different particles under NIR irradiation of 980 nm, MB was used as a model pollutant. Herein, 0.5 mg NaYF<sub>4</sub>:Yb,Tm@ZnO particles were dispersed in a 0.5 mL MB aqueous solution (15 mg L<sup>-1</sup>). Under NIR irradiation for 2 hours, 0.4 mL of MB aqueous solution was extracted for absorbance measurement. Photocatalytic activities of pure NaYF<sub>4</sub>:Yb,Tm, ZnO and their physical mixture of NaYF<sub>4</sub>:Yb,Tm and ZnO (NaYF<sub>4</sub>:Yb,Tm/ZnO) were also tested in this way. Fig. 5 shows the photocatalytic activities of the as-prepared samples for the degradation of MB under NIR irradiation of 980 nm. As shown in Fig. 5(a), in the presence of the NaYF<sub>4</sub>:Yb,Tm@ZnO composites, the absorption spectra of MB with a peak at 664 nm decreases gradually with an increase in irradiation time; this obviously indicates the degradation of MB.

To investigate the origin of the photocatalytic activity of the NaYF<sub>4</sub>:Yb,Tm@ZnO composites, five parallel experiments were designed as follows: (1) the MB solution in the presence of ZnO was kept in the dark. (2) The pure MB solution was irradiated with NIR light of 980 nm. (3) The MB solution was irradiated with NIR light of 980 nm in the presence of NaYF<sub>4</sub>:Yb,Tm. (4) The MB solution was irradiated with NIR light of 980 nm in the

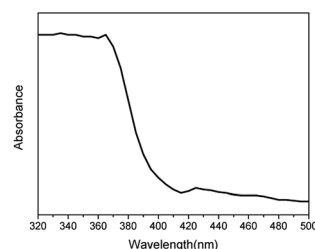


Fig. 4 UV-Vis absorbance spectra of NaYF<sub>4</sub>:Yb,Tm@ZnO composites.



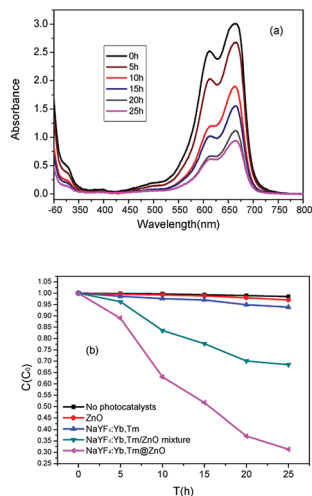


Fig. 5 (a) Absorbance spectra of MB catalyzed by the core-shell photocatalyst at different irradiation times under NIR excitation; (b) the time-dependent ratios of  $C/C_0$  in the presence of  $\text{NaYF}_4:\text{Yb,Tm@ZnO}$  core-shell composite and  $\text{NaYF}_4:\text{Yb,Tm/ZnO}$  physical mixture and with photocatalysts in the dark.

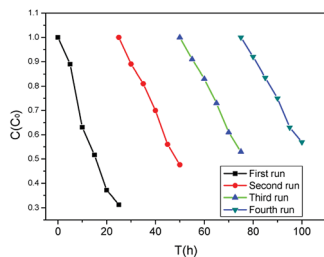


Fig. 6 Recyclability of the  $\text{NaYF}_4:\text{Yb,Tm@ZnO}$  core-shell composite under NIR light of 980 nm.

presence of the mixture of  $\text{NaYF}_4:\text{Yb,Tm/ZnO}$ . (5) The MB solution was irradiated with NIR light of 980 nm in the presence of the  $\text{NaYF}_4:\text{Yb,Tm@ZnO}$  composites. Then, the time-dependent rates of  $C/C_0$  were detected for different samples, as shown in Fig. 5b. The  $C_0$  is the primary concentration of MB and the  $C$  is the concentration of MB irradiated with the irradiation of 980 nm laser or in the dark at the time  $t$ ; the first experiment indicates a very small variation of the concentration of MB under the dark condition, as shown in Fig. 5b. It means that almost no degradation of MB occurred in the solution with ZnO in the dark. The same result was observed in the pure MB solution, and only 6% of MB was decomposed in the solution with  $\text{NaYF}_4:\text{Yb,Tm}$  irradiated by 980 nm for 10 h according to the change in concentration. As is known, NIR irradiation and nonradiative relaxations of excited  $\text{Yb}^{3+}$  and  $\text{Tm}^{3+}$  ions can generate thermal energy. The results obtained in the above-mentioned experiments indicate that the thermal energy generated by NIR irradiation or under the dark condition is not high enough to induce thermal degradation of MB appreciably. The  $\text{NaYF}_4:\text{Yb,Tm@ZnO}$  composite and  $\text{NaYF}_4:\text{Yb,Tm/ZnO}$  mixture exhibit strong photocatalytic activity, resulting in 68.7% and 37% degradation of MB after irradiation for 10 h,

respectively. This could be explained by their energy migration routes, as has been discussed in the photoluminescence section. The upconversion luminescence of  $\text{NaYF}_4:\text{Yb,Tm@ZnO}$  decreases significantly when compared with that of the  $\text{NaYF}_4:\text{Yb,Tm/ZnO}$  mixture. As  $\text{NaYF}_4:\text{Yb,Tm}$  and ZnO attach closely to each other and form compact interfaces, the core-shell-structured particles benefit FRET processes, whereas the  $\text{NaYF}_4:\text{Yb,Tm/ZnO}$  mixture has no contact interfaces between  $\text{NaYF}_4:\text{Yb,Tm}$  and ZnO particles, and then, ZnO can be excited mainly *via* radiation-reabsorption. Therefore, more NIR photon energy in the core-shell structure has been used to activate ZnO, and this results in high photocatalytic activity.

To assess the repeatability of near-infrared light-driven  $\text{NaYF}_4:\text{Yb,Tm@ZnO}$ , four consecutive photocatalytic experiments for the degradation of MB solution irradiated by NIR light of 980 nm for 12 h were studied. After each photocatalytic reaction,  $\text{NaYF}_4:\text{Yb,Tm@ZnO}$  was separated and washed with deionized water and ethanol several times for next run. Then, the time-dependent rates of  $C/C_0$  were detected for different runs. As shown in Fig. 6, about 68.7% of MB could be degraded for the first run and about 43% of MB is degraded in the fourth run; this indicated the good repeatability of the near-infrared light-driven photocatalytic activity of  $\text{NaYF}_4:\text{Yb,Tm@ZnO}$ .

## Conclusions

In this study, near-infrared core-shell structured  $\text{NaYF}_4:\text{Yb,Tm@ZnO}$  photocatalysts were prepared by a two-step high-temperature thermolysis method. XRD, TEM, the UV-vis spectra, and the PL spectra were used to characterize the photocatalytic material. The degradation of MB exposed to  $\text{NaYF}_4:\text{Yb,Tm@ZnO}$  core-shell particles upon NIR radiation demonstrated the NIR-driven photocatalytic capability. Compared with  $\text{NaYF}_4:\text{Yb,Tm}$ , ZnO, and the mixture of  $\text{NaYF}_4:\text{Yb,Tm}$  and ZnO, the  $\text{NaYF}_4:\text{Yb,Tm@ZnO}$  composite showed a significantly improved catalytic activity in the degradation of MB under 980 nm irradiation. This study suggests a promising system to research NIR photocatalysis, which may have an important implication on the utilization of solar energy.

## Conflicts of interest

There are no conflicts to declare.

## Acknowledgements

The authors thank the National Natural Science Foundation of China under Grant No. 61575019, 51272022 and 11474018.

## References

- G. Wang, Y. Ling and Y. Li, Oxygen-deficient metal oxide nanostructures for photoelectrochemical water oxidation and other applications, *Nanoscale*, 2012, 4(21), 6682–6691.
- Y. Tang, *et al.*, NIR-responsive photocatalytic activity and mechanism of  $\text{NaYF}_4:\text{Yb,Tm@TiO}_2$  core-shell nanoparticles, *ACS Catal.*, 2013, 3(3), 405–412.



- 3 A. Fujishima and K. Honda, Electrochemical photolysis of water at a semiconductor electrode, *nature*, 1972, **238**(5358), 37.
- 4 M. R. Hoffmann, *et al.*, Environmental applications of semiconductor photocatalysis, *Chem. Rev.*, 1995, **95**(1), 69–96.
- 5 A. L. Linsebigler, G. Lu and J. T. Yates Jr, Photocatalysis on TiO<sub>2</sub> surfaces: principles, mechanisms, and selected results, *Chem. Rev.*, 1995, **95**(3), 735–758.
- 6 M. A. Fox and M. T. Dulay, Heterogeneous photocatalysis, *Chem. Rev.*, 1993, **93**(1), 341–357.
- 7 X. Chen and S. S. Mao, Titanium dioxide nanomaterials: synthesis, properties, modifications, and applications, *Chem. Rev.*, 2007, **107**(7), 2891–2959.
- 8 C. Zhou, *et al.*, Effect of defects on photocatalytic dissociation of methanol on TiO<sub>2</sub> (110), *Chem. Sci.*, 2011, **2**(10), 1980–1983.
- 9 S. Hoang, *et al.*, Enhancing Visible Light Photo-Oxidation of Water with TiO<sub>2</sub> Nanowire Arrays *via* Cotreatment with H<sub>2</sub> and NH<sub>3</sub>: Synergistic Effects between Ti<sup>3+</sup> and N, *J. Am. Chem. Soc.*, 2012, **134**(8), 3659–3662.
- 10 W. Qin, *et al.*, Near-infrared photocatalysis based on YF<sub>3</sub>:Yb<sup>3+</sup>, Tm<sup>3+</sup>/TiO<sub>2</sub> core/shell nanoparticles, *Chem. Commun.*, 2010, **46**(13), 2304–2306.
- 11 J. Zhang, *et al.*, Near-infrared light-induced photocatalysis of NaYF<sub>4</sub>:Yb, Tm@Cu<sub>2</sub>O core-shell nanocomposites, *Opt. Mater.*, 2018, **84**, 89–93.
- 12 S. Cho, *et al.*, Porous ZnO–ZnSe nanocomposites for visible light photocatalysis, *Nanoscale*, 2012, **4**(6), 2066–2071.
- 13 D. Chen, *et al.*, Preparation and enhanced photoelectrochemical performance of coupled bicomponent ZnO–TiO<sub>2</sub> nanocomposites, *J. Phys. Chem. C*, 2008, **112**(1), 117–122.
- 14 Z. Liu, *et al.*, Photocatalytic degradation of gaseous benzene with CdS-sensitized TiO<sub>2</sub> film coated on fiberglass cloth, *J. Mol. Catal. A: Chem.*, 2012, **363**, 159–165.
- 15 D. I. Son, *et al.*, High efficiency ultraviolet photovoltaic cells based on ZnO–C 60 core–shell QDs with organic–inorganic multilayer structure, *J. Mater. Chem.*, 2012, **22**(3), 816–819.
- 16 L. Sun, *et al.*, A white-emitting ZnO–Au nanocomposite and its SERS applications, *Appl. Surf. Sci.*, 2012, **258**(20), 7813–7819.
- 17 Y. Bessekhoud, D. Robert and J. Weber, Bi<sub>2</sub>S<sub>3</sub>/TiO<sub>2</sub> and CdS/TiO<sub>2</sub> heterojunctions as an available configuration for photocatalytic degradation of organic pollutant, *J. Photochem. Photobiol., A*, 2004, **163**(3), 569–580.
- 18 W. Choi, A. Termin and M. R. Hoffmann, The role of metal ion dopants in quantum-sized TiO<sub>2</sub>: correlation between photoreactivity and charge carrier recombination dynamics, *J. Phys. Chem.*, 1994, **98**(51), 13669–13679.
- 19 L. Xu, E. M. Steinmiller and S. E. Skrabalak, Achieving synergy with a potential photocatalytic Z-scheme: synthesis and evaluation of nitrogen-doped TiO<sub>2</sub>/SnO<sub>2</sub> composites, *J. Phys. Chem. C*, 2011, **116**(1), 871–877.
- 20 H.-Y. Chuang and D.-H. Chen, Fabrication and photocatalytic activities in visible and UV light regions of Ag@TiO<sub>2</sub> and NiAg@TiO<sub>2</sub> nanoparticles, *Nanotechnology*, 2009, **20**(10), 105704.
- 21 F. Wang and X. Liu, Recent advances in the chemistry of lanthanide-doped upconversion nanocrystals, *Chem. Soc. Rev.*, 2009, **38**(4), 976–989.
- 22 G. Chen, *et al.*, Ultrasmall monodisperse NaYF<sub>4</sub>: Yb<sup>3+</sup>/Tm<sup>3+</sup> nanocrystals with enhanced near-infrared to near-infrared upconversion photoluminescence, *ACS Nano*, 2010, **4**(6), 3163–3168.
- 23 C. Li, *et al.*, NaYF<sub>4</sub>: Yb, Tm/CdS composite as a novel near-infrared-driven photocatalyst, *Appl. Catal., B*, 2010, **100**(3–4), 433–439.
- 24 D.-X. Xu, *et al.*, Advanced near-infrared-driven photocatalyst: Fabrication, characterization, and photocatalytic performance of β-NaYF<sub>4</sub>:Yb<sup>3+</sup>, Tm<sup>3+</sup>@TiO<sub>2</sub> core@shell microcrystals, *Appl. Catal., B*, 2013, **142–143**, 377–386.
- 25 W. Wang, *et al.*, A NIR-driven photocatalyst based on α-NaYF<sub>4</sub>:Yb,Tm@TiO<sub>2</sub> core–shell structure supported on reduced graphene oxide, *Appl. Catal., B*, 2016, **182**, 184–192.
- 26 M. Z. Huang, *et al.*, Toward NIR driven photocatalyst: Fabrication, characterization, and photocatalytic activity of beta-NaYF<sub>4</sub>:Yb(3+),Tm(3+)/g-C<sub>3</sub>N<sub>4</sub> nanocomposite, *J. Colloid Interface Sci.*, 2015, **460**, 264–272.
- 27 X. Guo, *et al.*, Near-infrared photocatalysis of β-NaYF<sub>4</sub>: Yb<sup>3+</sup>, Tm<sup>3+</sup>@ZnO composites, *Phys. Chem. Chem. Phys.*, 2013, **15**(35), 14681–14688.
- 28 L. Wang, *et al.*, Enhanced energy transfer in heterogeneous nanocrystals for near infrared upconversion photocurrent generation, *Nanoscale*, 2017, **9**(47), 18661–18667.
- 29 F. Vetrone, *et al.*, Concentration-dependent near-infrared to visible upconversion in nanocrystalline and bulk Y<sub>2</sub>O<sub>3</sub>: Er<sup>3+</sup>, *Chem. Mater.*, 2003, **15**(14), 2737–2743.

